www.nature.com/aps

Acta Pharmacologica Sinica

ARTICLE

Osthole inhibits the migration and invasion of highly metastatic breast cancer cells by suppressing ITGα3/ITGβ5 signaling

Yue-qiang Chen[1], Hai-yan Song[2], Zhong-yan Zhou[1], Jiao Ma[1], Zhan-yang Luo[1], Ying Zhou[3], Jian-yi Wang[4], Sheng Liu[1] and Xiang-hui Han[1]

Metastasis is the leading cause of death in breast cancer patients. Osthole, as an active compound detected in the traditional Chinese medicine Wenshen Zhuanggu Formula, has shown a promising anti-metastatic activity in human breast cancer cells, but the underlying mechanisms remain ambiguous. In this study we elucidated the anti-metastatic mechanisms of osthole in highly metastatic breast cancer cells and a zebrafish xenograft model. We showed that the expression of integrin α3 (ITGα3) and integrin β5 (ITGβ5) was upregulated in highly metastatic MDA-MB-231, MDA-MB-231BO breast cancer cell lines but was downregulated in poorly metastatic MCF-7 breast cancer cell line, which might be the key targets of osthole's anti-metastatic action. Furthermore, we showed that knockdown of ITGα3 and ITGβ5 attenuated breast cancer cell migration and invasion possibly via suppression of FAK/Src/Rac1 pathway, whereas overexpression of ITGα3 and ITGβ5 caused the opposite effects. Consistently, osthole significantly inhibited breast cancer metastasis by downregulating ITGα3/ITGβ5 signaling in vitro and in vivo. These results provide new evidence that osthole may be developed as a candidate therapeutic drug for metastatic breast cancer.

Keywords: osthole; Wenshen Zhuanggu Formula; breast cancer; metastasis; ITGα3; ITGβ5; FAK/Src/Rac1 pathway

Acta Pharmacologica Sinica (2022) 43:1544–1555; https://doi.org/10.1038/s41401-021-00757-7

INTRODUCTION

In 2020, breast cancer has become the most frequent cancer worldwide, with 11.7% of the total new cases (19.3 million) and 6.9% of the total cancer deaths (9.9 million), respectively. Among women, breast cancer accounts for 1 in 5 cancer cases and for 1 in 10 cancer deaths, ranking first for incidence and fourth for mortality in China [1]. Metastasis is the major leading cause of death in breast cancer patients. Approximately 90% of cancer-related deaths are attributed to metastasis, and the 5-year overall survival rate for metastatic breast cancer patients is less than 40% [2]. Breast cancer mainly metastasizes to the bone, lung, liver, and brain via the circulation. The most frequent site of breast cancer metastasis is the bone, which occurs in about 80% of patients with advanced disease [3]. Conventional treatments for breast cancer metastasis include standard chemotherapy, hormone therapy, immunological therapy and antiangiogenic therapy [4]. However, these methods are still not very effective in preventing relapses and in the management of breast cancer metastasis [5]. In order to improve long-term survival of the patients with breast cancer, it is essential to explore the molecular mechanisms of the metastatic signaling pathways and develop novel drugs in addition to current treatments.

Integrins are a large family of heterodimeric transmembrane glycoproteins that mediate cell-cell and cell-cellular environment interactions [6]. Integrins are composed of α and β subunits and widely expressed in many types of cells including cancer cells and other normal cells [7–9]. In cancer cells, integrins serve as a receptor for adhesion proteins and growth factors in the extracellular matrix (ECM) to mediate tumor cell attachment, invasion, migration, and tumor angiogenesis [10]. Various integrins such as α2β1, α3β1, α5β1, α6β1, αvβ3, αvβ5, αvβ6, and α6β4, have been found to be highly expressed in breast cancer cells [11]. Integrins promote breast cancer metastasis by initiating focal adhesion kinase (FAK)/Src/Rac1 tyrosine phosphorylation cascade. Huang et al. found that integrin α5 along with δ-catenin mediated FAK signaling pathway to stimulate Rac1-mediated cell migration and movement in human primary and lymph node metastatic breast cancer [12]. Flamini et al. reported that integrin αvβ3 triggered the process of FAK phosphorylation and translocation at sites where focal adhesion complexes controlled by T3 in breast cancer T-47D cells [13]. Tai et al. described that the concomitant overexpression of Src-dependent integrin β4 and FAK significantly correlates with malignant potential in patients with triple-negative breast cancer (TNBC) [14]. Li et al. elucidated

[1]Institute of Chinese Traditional Surgery, Longhua Hospital Affiliated to Shanghai University of Traditional Chinese Medicine, Shanghai 200032, China; [2]Institute of Digestive Diseases, Longhua Hospital Affiliated to Shanghai University of Traditional Chinese Medicine, Shanghai 200032, China; [3]Shanghai TCM-integrated Hospital Affiliated to Shanghai University of Traditional Chinese Medicine, Shanghai 200082, China and [4]Department of Liver Disease, Shuguang Hospital Affiliated to Shanghai University of Traditional Chinese Medicine, Shanghai 201203, China
Correspondence: Jian-yi Wang (wjydyj@163.com) or Sheng Liu (lshtcm@126.com) or Xiang-hui Han (hanxianghui1106@163.com)
These authors contributed equally: Yue-qiang Chen, Hai-yan Song

Received: 1 April 2021 Accepted: 2 August 2021
Published online: 23 August 2021

that the expression and activity of the downstream kinases of integrin β6 promoted FAK/Src interaction and the invasion and migration of breast cancer MCF-7 cells [15].

In China, traditional Chinese medicine (TCM) formula and its active components are used extensively to treat breast cancer bone metastasis as an adjuvant therapy in combination with other treatment modalities; this treatment can effectively relieve bone pain, reduce the incidence of SRE, and improve the quality of life in patients [16]. A randomized, double-blind, and controlled trial revealed that Wenshen Zhuanggu Formula (WSZG) combined with radiotherapy exerted favorable therapeutic effects against bone metastasis in breast cancer patients [17]. WSZG significantly decreased the incidence of bone metastases and protected against bone lesions in a mouse xenograft model induced by MDA-MB-231BO breast cancer cells [18]. Subsequently, six coumarin components (psoralen, isopsoralen, bergapten, xanthotoxin, osthole, and imperatorin) were detected through liquid chromatography tandem mass spectrometry in whole blood of breast cancer bone metastatic mice following oral administration of WSZG extract [19]. Accumulating studies have shown that these coumarins, especially osthole, exert anticancer, antiinflammatory, antioxidant, and antibacterial activities [20–23].

Osthole, 7-methoxy-8-(3-methyl-2-butenyl) coumarin derived from *Cnidium monnieri* (L.) Cusson, is known to possess promising anticancer effects against multiple cancer types including breast, lung, hepatic, prostate, and ovarian cancer [24]. For breast cancer, osthole exhibits low cytotoxicity to normal cells, but may target heterogenous cancer cells and multiple signaling pathways. One previous study found that osthole induced cell apoptosis by activating the phosphorylation of Akt, ERK1/2, and JNK proteins in breast cancer BT-474 and MCF-7 cells [25]. Another study reported that osthole suppressed the proliferation of TNBC cells by blocking STAT3 signaling pathway [26]. Additionally, osthole inhibited the migration, invasion and EMT of breast cancer MCF-7 and MDA-MB-231 cells by targeting MMP2 protein and HGF/c-Met signaling pathway [27, 28]. Yet to date, the anti-metastatic effects of osthole and its underlying mechanisms have not been fully elucidated.

The present study aimed to explore the anti-metastatic mechanisms of osthole in breast cancer cells and zebrafish xenograft model. We first screened and validated the osthole-targeted integrin α3 and β5 (ITGα3 and ITGβ5). And then we investigated whether osthole attenuated the invasion and migration of highly metastatic breast cancer cells by regulating integrin-triggered FAK/Src signaling pathway.

MATERIALS AND METHODS

Chemicals and reagents

Osthole, xanthotoxin, and isopsoralen (Lot. wkq17061204, wkq17061203, wkq17061604, purity > 98%) were purchased from Sichuan WeiKeqi Biological Technology Co., Ltd. (Chengdu, China). Rabbit anti-human antibodies for integrin β5 (ITGβ5, catalog #3629), FAK (catalog #71433), phospho-FAK (p-FAK, catalog #8556), HSP70 (catalog #4873), Src (catalog #2108), phospho-Src (p-Src, catalog #2105), phospho-paxillin (p-PXN, catalog #2541), and moesin (MSN, catalog #3150) were acquired from Cell Signaling Technology, Inc. (Danvers, MA, USA). Rabbit anti-human antibodies for integrin α3 (ITGα3, ab131055), S100A (ab11428), paxillin (PXN, ab32084) and Rac1 mouse anti-human antibody (ab33186) were obtained from Abcam Trading (Shanghai) Co., Ltd. (China). Rabbit anti-human antibodies for integrin αv (ITGαv, DF6815) and integrin α2 (ITGα2, DF2540) were purchased from Affinity Biosciences, Ltd. (Cincinnati, OH, USA). N-cadherin rabbit anti-human antibody (22018-1-A-P), E-cadherin mouse anti-human antibody (60335-1-Ig), and β-actin mouse anti-human antibody (66009-1-Ig) were acquired from Proteintech Group, Inc. (Rosemont, IL, USA). The secondary antibodies including anti-rabbit and anti-mouse IgG linked to horseradish peroxidase (HRP, Cat. No. D110058-0025 and AS003), anti-rabbit and anti-mouse IgG conjugated to Alexa Flour 488 (catalog #4412 and catalog #4408) were provided by Sangon Biotech (Shanghai) Co., Ltd. (China) and Cell Signaling Technology, respectively. All other reagents were of analytical grade.

Cell lines

Human breast cancer cell lines MCF-7, MDA-MB-231, T-47D, SK-Br-3 (Institute of Biochemistry and Cell Biology, Chinese Academy of Sciences, Shanghai, China), MDA-MB-231BO (a gift from Dr. Toshiyuki Yoneda, Texas State University, San Marcos, TX, USA) and lentivirus packaging cells (HEK293T, American Type Culture Collection, Manassas, VA, USA) were maintained in Dulbecco's modified Eagle's medium (DMEM)/high glucose with 10% fetal bovine serum (FBS). Human normal mammary epithelial MCF-10A cell lines (Institute of Biochemistry and Cell Biology, Chinese Academy of Sciences, Shanghai, China) were maintained with special medium including DMEM/F12, 5% horse serum, 20 ng/mL epidermal growth factor, 0.5 μg/mL hydrocortisone, 10 μg/mL insulin, 1% nonessential amino acid, and 1% penicillin/streptomycin. All cell lines were cultured at 37 °C in a humidified atmosphere containing 5% CO_2.

Cell proliferation, migration, and invasion assay

For proliferation assay, MDA-MB-231, MDA-MB-231BO, MCF-7 breast cancer cells and MCF-10A mammary epithelial cells (5×10^3/well) were seeded into 96-well plates and cultured overnight. The cells were incubated with 0.1% dimethyl sulfoxide (DMSO, as control) or osthole (2, 5, 10, 25, and 50 μg/mL), xanthotoxin (5, 10, 20, 40, and 80 μg/mL), and isopsoralen (5, 10, 25, 50, and 100 μg/mL) for 24 or 48 h. Cell viability was then detected by sulforhodamine B (SRB) assay, and the IC_{50} value for each drug was calculated by fitting a four-parameter dose-response curve to normalized data using GraphPad Prism7.0 software. For migration assay, three types of breast cancer cells (5×10^5/well) were seeded in 6-well plates and cultured overnight until 80%–90% confluence. Monolayer cells were scratched in a straight line with a 1 mL pipette tip and then treated with 0.1% DMSO (as control), 25 μg/mL of osthole, xanthotoxin, or isopsoralen for 24 or 48 h. After treatment, cells were taken with an Olympus IX71 microscope (Olympus Co., Tokyo, Japan) at different time points (0, 24, and 48 h). For invasion assay, 5×10^4/well of MDA-MB-231 and MDA-MB-231BO cells were treated with 25 μg/mL of osthole, xanthotoxin, or isopsoralen for 24 or 48 h. The cells were subsequently seeded in the Matrigel-coated upper chambers (8 μm pore size; Corning Costar, Cambridge, MA, USA) and permitted to invade to the lower chamber containing DMEM with 5% FBS for 20 h. After the chambers were fixed with 4% paraformaldehyde and stained with crystal violet, the number of invading cells was counted in five random fields of view (200× magnification) under a microscope. All the above assays were repeated three times.

Ethic statement

Zebrafish were provided by Prof. Simon Lee from University of Macau and maintained by the Laboratory Animal Service Center, Longhua Hospital, Shanghai University of Traditional Chinese Medicine. All zebrafish experimental procedures were approved by the Longhua Hospital-Animal Experimentation Ethics Committee of Shanghai University of Traditional Chinese Medicine.

Zebrafish maintenance and embryo handling

Zebrafish maintenance was performed according to the Zebrafish Handbook (Westerfield, 2007). In brief, zebrafishes were kept separately under a 14 h light and 10 h dark cycle and fed brine shrimp twice a day. Zebrafish embryos were generated by natural pairwise mating and incubated at 28.5 °C in embryo medium. After 24 h of incubation, chorions were removed with a sharp

forceps, and health development embryos were selected for later use.

Zebrafish breast cancer xenotrasplantation model and drug treatment

In accordance with the previously described method [29], zebrafish embryos were anesthetized in 0.04 mg/mL tricaine (Sigma-Aldrich (Shanghai) Trading Co., Ltd, China) and then 2 μL CM-Dil-labeled MDA-MB-231BO breast cancer cells were injected into the perivitelline cavity of each embryo. After confirmation of a visible cell mass at the injection site, zebrafish embryos were transferred to a 24-well microplate with 10 fish in each well and treated with different concentrations of osthole (3, 10, and 20 μmol/L) for 48 h. Zebrafish embryos treated with embryo medium or PBS solution containing 0.1% DMSO were used as blank control or vehicle control, respectively. At the treatment endpoint, zebrafish were embedded in a lateral orientation in 0.5% agarose. Images of the tumor cells throughout the fish were captured using an inverted fluorescence microscope (Eclipse Ti-U, Nikon Corp., Tokyo, Japan). Mean fluorescence intensity (MFI) of tumor cells was analyzed on ImageJ software.

Real-time polymerase chain reaction (real-time PCR)

The total RNA of zebrafish and tumor cells was isolated with TRIzol reagent (Invitrogen, Life Technologies Corp., Grand Island, NY, USA). Reverse transcription of the synthesized cDNA was performed with a ReverTra Ace qPCR RT Kit (Toyobo Co., Osaka, Japan). The resulting cDNA was subjected to real-time PCR for 1 cycle at 95 °C for 60 s followed by up to 40 cycles of 95 °C for 15 s, 60 °C for 15 s, and 72 °C for 45 s with SYBR Green Master Mix (Takara Bio. Inc., Osaka, Japan). The mRNA level was quantified with the QuantStudio 3 Real-Time PCR system (Applied Biosystems, Foster City, CA, USA). The relative expression level of RNAs was analyzed by using $2^{-\Delta\Delta CT}$ method. The sequences of primers used are listed in Table 1.

Western blot analysis

Total protein (35 μg) from cell lysates was collected. Samples in different groups ($n = 3$) were separated on 8% or 10% sodium dodecyl sulfate-polyacrylamide gel electrophoresis (Invitrogen, Life Technologies Corp., Grand Island, NY, USA) and transferred to polyvinylidene difluoride membranes (0.2 μm). After blocking with 5% fat-free milk for 1 h, the membranes were incubated at 4 °C overnight with the primary antibodies for FAK, p-FAK, Src, p-Src, PXN, p-PXN, Rac1, MSN, S100A, HSP70, N-cadherin, E-cadherin, ITGβ5, ITGα3, ITGα2, ITGαv, and β-actin. All primary antibodies were diluted to working concentrations (1:1000) in the antibody diluent (Beyotime Biotechnology Co. Ltd., Shanghai, China). The membranes incubated for 2 h at room temperature with the appropriate HRP-conjugated secondary antibodies (1:5000), before washed three times with TBST. Protein bands were exposed using an efficient chemiluminescence kit (Millipore Corp., Billerica, MA, USA) and visualized with ChemiDoc™ Imaging Systems (Bio-Rad Laboratories Inc., Hercules, CA, USA).

RNA sequencing

MDA-MB-231BO cells were treated with 10 μg/mL osthole for 48 h. The total RNA in control and osthole-treated groups was extracted by using TRIzol method. The concentration and purity of total RNA were measured with NanoDrop 2000 (Thermo Fisher Scientific Inc., Waltham, MA, USA). The integrity of RNA samples was measured with an Agilent 2100 Bioanalyzer. Total RNA samples were submitted for second-generation sequencing technology analysis service using Illumina NovaSeq (Shanghai Personal Biotechnology Co., Ltd, China). Briefly, paired-end method was applied for RNA sequencing and the read length was 150 base pair. To identify differentially expressed genes (DEGs) between osthole-treated group relative to control, we used "DESeq" package in R with the following screening criteria: |log2 Fold Change| > 1 and adjusted P value < 0.05. The DEGs in each treatment group were submitted for functional enrichment analyses of heat map and Kyoto Encyclopedia of Genes and Genomes (KEGG) pathways.

Table 1. Sequences of forward and reverse primers used in real-time PCR analysis.

Genes	Sequences
β-actin	Forward: 5′-TGACGTGGACATCCGCAAAG-3′ Reverse: 5′-CTGGAAGGTGGACAGCGAGG-3′
ITGαv	Forward: 5′-AACCCAAGCTGGAAGTTTCTG-3′ Reverse: 5′-GCAGTGGAATGGAAACGATG-3′
ITGα2	Forward: 5′-GGACTTTCGCATCATCAACG-3′ Reverse: 5′-GGTACTTCGGCTTTCTCATCAG-3′
ITGα3	Forward: 5′-ACCCCAACTACAGGCGAAAC-3′ Reverse: 5′-AGAAGAAGCCGTGGAAGACAG-3′
ITGβ5	Forward: 5′-ATCCCTTGCCTTGCTTGG-3′ Reverse: 5′-CACCGTTGTTCCAGGTATCAG-3′
FAK	Forward: 5′-CAGCTCAGCACAATCCTGGAG-3′ Reverse: 5′-TTCGCTGGACCTCGGACTG-3′
Src	Forward: 5′-CTTTGGCGAGGTGTGGATG-3′ Reverse: 5′-GTAAATGGGCTCCTCTGAAACC-3′
Rac1	Forward: 5′-GGCACCACTGTCCCAACAC-3′ Reverse: 5′-GCACTCCAGGTATTTTACAGCAC-3′
Paxillin	Forward: 5′-CTTTGGTCCCGAAGGGTTC-3′ Reverse: 5′-AGGATGCCACAGCGTGTTG-3′
HSP70	Forward: 5′-ACTGTGGACCTGCCAATCG-3′ Reverse: 5′-GCATCATTCCGCTCCTTCTC-3′
Moesin	Forward: 5′-TTAAGTTCCGTGCCAAGTTCTAC-3′ Reverse: 5′-AGGCGGGCAGTAAATATCATC-3′
S100A	Forward: 5′-CCCTCATCAACGTGTTCCAC-3′ Reverse: 5′-CATCACCTTGTCCACAGCATC-3′

Plasmid construction, shRNA, and viral infection

Human wild-type cDNA or shRNA sequences of ITGα3 or ITGβ5 were cloned into the pcDH-puro or pLKO.1-puro vectors to enhance or knock down the expression target genes. The pcDH-ITGα3, pcDH-ITGβ5, pcDH, pLKO.1-ITGα3, pLKO.1-ITGβ5, and pLKO.1 vectors were cotransfected into HEK293T cells by using a packaging system, including pSPAX2 and pMD2G vector to produce lentiviral particles. After removing all media, viruses were collected at 24, 48, and 72 h and filtered with a 0.45-mm filter lip after centrifugation at 1000 r/min for 5 min at 4 °C. MCF-7, MDA-MB-231, and MDA-MB-231BO cells were infected at 70% density for 24 h and the positive clones were selected with puromycin (3 μg/mL) for 14 d to establish the ITGα3 or ITGβ5 overexpression and knockdown cell lines. The sequences for constructing shRNA were obtained from Sigma-Aldrich. They are provided in Table 2.

Confocal immunofluorescence

MDA-MB-231BO, MDA-MB-231BO and MCF-7 cells were separately treated with 10 μg/mL osthole for 48 h. Different breast cancer cells (MDA-MB-231: 7×10^4/well, MDA-MB-231BO: 1.5×10^5/well, MCF-7: 3×10^5/well) were seeded on a glass-bottomed cell culture dish and fixed with 4% paraformaldehyde. After permeabilization with 0.3% Triton-X 100 and blocked with 5% bovine serum albumin for 30 min, the cells were incubated with primary antibodies against FAK, p-FAK, Src, PXN, p-PXN, Rac1, HSP70, MSN, and S100A at concentrations of 1:50-1:300, at 4 °C overnight. The cells were then washed three times with PBS, and the secondary antibodies (anti-rabbit or anti-mouse IgG conjugated to Alexa Flour 488, 1:500) were incubated at room temperature for 1 h. The cells were stained with DAPI (1:5000) for 5 min. Images were captured via confocal immunofluorescence microscopy (LSM-800,

Table 2. Target sequences of ITGα3 and ITGβ5 for constructing lentiviral shRNA.

Genes	Sequences
ITGα3	Sense: 5′-GCUACAUGAUUCAGCGCAAdTdT-3′ Antisense: 5′-UUGCGCUGAAUCAUGUAGCdTdT-3′
ITGβ5	Sense: 5′-CUUUCUGUGAGUGCGACAAdTdT-3′ Antisense: 5′-UUGUCGCACUCACAGAAAGdTdT-3′
Control	Sense: 5′-UUCUCCGAACGUGUCACGUdTdT-3′ Antisense: 5′-ACGUGACACGUUCGGAGAAdTdT-3′

Carl Zeiss AG, Oberkochen, Germany). The MFI of immunofluorescence images for each target protein was measured by dividing the integrated density values with the total surface area following thresholding on ImageJ software.

Statistics

Data are presented as mean ± SD. Analysis of variance (ANOVA) was used for multiple comparisons, and Fisher's LSD test or Games-Howell test was used for the comparison of two means. A value of $P < 0.05$ was considered statistically significant.

RESULTS

Comparison of the anticancer effects of three components from WSZG extract

Osthole, xanthotoxin and isopsoralen were isolated from WSZG extract and identified as three major chemical components. The antitumor activities of these components against human breast cancer cells (MDA-MB-231, MDA-MB-231BO, and MCF-7 cells) were investigated via SRB, wound healing, and transwell assays. SRB assay showed that the three components significantly inhibited the viability of different cells after treatment for 24 and 48 h ($P < 0.05$ or $P < 0.01$, Fig. 1a). Osthole with IC_{50} values of 24.2, 6.8, and 123.9 μg/mL (48 h) against MDA-MB-231, MDA-MB-231BO, and MCF-7 cells, respectively, demonstrated superior activities to isopsoralen, and xanthotoxin. Besides, osthole displayed a lower cytotoxicity than isopsoralen, and xanthotoxin against normal MCF-10A cells with the IC_{50} value of 8944.0 μg/mL (Fig. 1a, Table 3).

Wound healing assay showed that the migration speed of three breast cancer cells was significantly reduced after 24- and 48-h incubation with 25 μg/mL of osthole, isopsoralen or xanthotoxin ($P < 0.01$). For 48 h treatment, osthole reduced the migration rate of the MDA-MB-231, MDA-MB-231BO, and MCF-7 cells to 8.05%, 15.71%, and 35.70%, respectively. By comparison, isopsoralen and xanthotoxin decreased the migration rate of three breast cancer cells to 21.25%, 26.99%, 37.06% and 36.63%, 31.29%, 51.08% (Fig. 1b). For Transwell assay, 25 μg/mL of osthole and isopsoralen treatment for 24 and 48 h remarkably suppressed the invasive potential of MDA-MB-231BO and MDA-MB-231 cells ($P < 0.05$ or $P < 0.01$), whereas 25 μg/mL of xanthotoxin had no influence on the cell invasion ($P > 0.05$). The number of invading cells treated with osthole or isopsoralen for 48 h decreased by 49.3% or 12.2% (MDA-MB-231 cells) and 39.3% or 2.7% (MDA-MB-231BO cells), respectively (Fig. 1c). These results indicated that osthole had superior antiproliferative and antimetastatic effects on multiple breast cancer cells and lower cytotoxicity to normal mammary epithelial cells compared with the two other components.

Osthole inhibits breast cancer metastasis in vitro and in vivo

High-metastatic MDA-MB-231 and its bone-tropic MDA-MB-231BO breast cancer cells were treated with 5, 10, and 25 μg/mL osthole for 24 and 48 h. SRB assay showed that osthole effectively reduced the cell viability in a dose- and time-dependent manner compared with controls (Fig. 2a). Wound healing assay revealed that osthole exposure significantly decreased the migration rate of the two breast cancer cells in a dose-dependent manner (Fig. 2b). Transwell assay indicated that osthole treatment caused a significant and dose-dependent decrease in the invasion ability of MDA-MB-231 and MDA-MB-231BO cells (Fig. 2c).

To exclude the influence of cancer cell proliferation on motility and metastasis, MDA-MB-231BO and MDA-MB-231 cells were treated with mitomycin C (10 μg/mL) for 2 h to inhibit cell proliferation prior to the wound-healing and Transwell assays. Consistent with above results, 5, 10, and 25 μg/mL of osthole treatment for 24 and 48 h dramatically impaired the migratory and invasive abilities of two metastatic breast cancer cells with mitomycin C pre-treatment (Supplementary Fig. S1).

A zebrafish breast cancer xenograft model was established to assess the anti-metastatic activity of osthole in vivo. As shown in Fig. 2d, the highly metastatic MDA-MB-231BO cells in the untreated group widely spread away from the primary microinjection site of the zebrafish after CM-DiI stained tumor cells were injected into the perivitelline cavity of 48 hpf embryos. Osthole dose-dependently decreased the MFI of disseminated tumor cells in the zebrafish body compared with the untreated (blank) groups (3, 10, and 20 μmol/L of osthole-treated groups *vs* the blank group: 20.90 ± 0.24, 18.24 ± 0.12, and 17.44 ± 0.31 *vs.* 35.78 ± 0.89; $P < 0.01$).

We also analyzed the effect of osthole on the epithelial marker E-cadherin and the mesenchymal markers HSP70, MSN, S100A, and N-cadherin in highly metastatic breast cancer cells. Western blot analysis showed that various concentrations of osthole (5, 10, and 25 μg/mL) significantly upregulated the protein expression of E-cadherin and downregulated the protein expression of HSP70, MSN, S100A, and N-cadherin in MDA-MB-231 and MDA-MB-231BO cells ($P < 0.05$ or $P < 0.01$, Fig. 2e). Real-time PCR analysis further demonstrated that 20 μmol/L of osthole significantly decreased the mRNA expression levels of HSP70, MSN, and S100A by 62.9%, 89.6%, and 86.1% in zebrafish-injected with MDA-MB-231BO cells, respectively ($P < 0.01$, Fig. 2e).

Additionally, we investigated the regulation of different doses of osthole on integrin downstream proteins like FAK, p-FAK, Src, p-Src, PXN, p-PXN, and Rac1 in highly metastatic breast cancer cells. The results of Western blot analysis showed that osthole efficiently inhibited the protein expression levels of p-FAK/total FAK, p-Src/total Src, p-PXN/total PXN and Rac1 in MDA-MB-231 and MDA-MB-231BO cells compared with the control group ($P < 0.05$ or $P < 0.01$, Fig. 2f).

Identification of candidate target genes of osthole in highly bone-metastatic breast cancer cells

RNA sequencing was used to analyze the expression profiles of untreated MDA-MB-231BO cells and osthole-treated MDA-MB-231BO cells and identified the target genes of osthole against breast cancer metastasis. There were a total of 847 DEGs between the two groups ($P < 0.05$, $|\log2 \text{ Fold Change}| > 1$), including 471 upregulated genes and 376 downregulated genes. KEGG enrichment analysis of the DEGs indicated that multiple cancer-related pathways were significantly involved in the action mechanisms of osthole, including DNA replication, TGF-beta signaling pathway, FoxO signaling pathway, ECM-receptor interaction, B cell receptor signaling pathway, apoptosis, ErbB signaling pathway, and p53 signaling pathway (Fig. 3a). Therein, ECM-receptor interaction was our key concerned signaling pathway due to its high relevance with tumor progression. From the heat map that showed significant targets in ECM-receptor interaction such as ITGαv, ITGα2, ITGα3, and ITGβ5 were significantly downregulated in osthole-treated cancer cells (Fig. 3b). Studies have shown that these integrin genes can activate ECM-mediated FAK signaling to couple cell-matrix interactions [10, 30]. In vitro validated assay further determined that ITGα3 and ITGβ5 might be the most significant candidate target genes regulated by osthole (Fig. 3c).

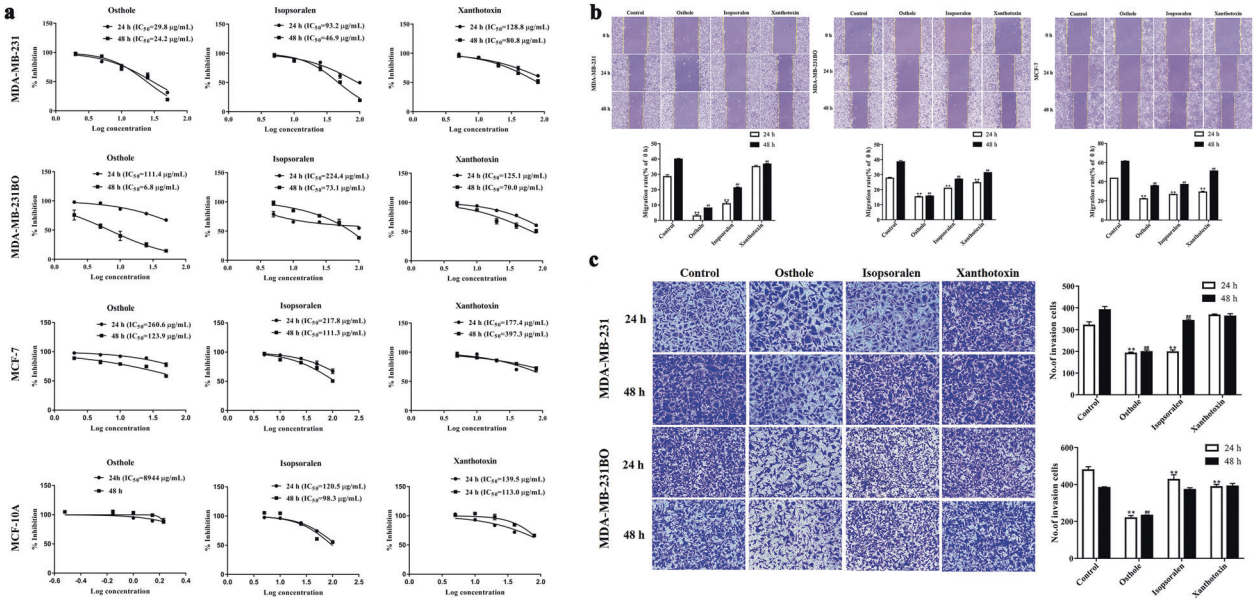

Fig. 1 Comparation of antitumor effects of isopsoralen, osthole, and xanthotoxin on different breast cancer cells. a SRB assay was performed to measure the effects of three components on cell viability of breast cancer cells (MDA-MB-231, MDA-MB-231BO, and MCF-7) and normal mammary epithelial MCF-10A cells. **b** Wound-healing assay was performed to detect the effects of three components (25 μg/mL) on cell migration of MDA-MB-231, MDA-MB-231BO, and MCF-7 breast cancer cells. **c** Transwell assay was performed to investigate the effects of three components (25 μg/mL) on cell invasion of MDA-MB-231 and MDA-MB-231BO breast cancer cells. Data were expressed as the mean ± SD for triplicate. $^{*}P < 0.05$, $^{**}P < 0.01$ *vs*. the control group for 24 h; $^{\#}P < 0.05$, $^{\#\#}P < 0.01$ *vs*. the control group for 48 h. Amplification factors: 100× for **b** and 200× for **c**.

Table 3. The IC_{50} values of MDA-MB-231, MDA-MB-231BO, MCF-7, and MCF-10A cells treated with osthole, isopsoralen, and xanthotoxin for 24 h or 48 h, respectively

IC_{50} (μg/mL)						
Cells	Osthole		Isopsoralen		Xanthotoxin	
	24 h	48 h	24 h	48 h	24 h	48 h
MDA-MB-231	29.8	24.2	93.2	46.9	128.8	80.8
MDA-MB-231BO	111.4	6.8	224.4	73.1	125.1	70.0
MCF-7	260.6	123.9	217.8	111.3	177.4	397.3
MCF-10A	8944.0	/	120.5	98.3	139.5	113.0

Subsequently, real-time PCR and Western blot analysis were conducted to examine whether osthole treatment (5, 10, and 25 μg/mL) directly downregulated ITGα3 and ITGβ5 in MDA-MB-231 and MDA-MB-231BO cells. The mRNA and protein expression levels of ITGα3 and ITGβ5 were significantly repressed in osthole-treated groups compared with the control group ($P < 0.05$ or $P < 0.01$, Fig. 3d). Similarly, 20 μmol/L of osthole significantly decreased the mRNA expression levels of ITGα3 and ITGβ5 in the zebrafish xenograft model induced by MDA-MB-231BO cells ($P < 0.01$, Fig. 3d).

Establishment of stable ITGα3 or ITGβ5 knockdown and overexpression in human breast cancer cells

Previous studies reported that integrins might play a key role in tumor progression [31]. To explore the effect of ITGα3 and ITGβ5 on the migration and invasion of breast cancer cells, we first analyzed the ITGα3 and ITGβ5 expression levels in five human breast cancer cell lines (two highly metastatic: MDA-MB-231 and MDA-MB-231BO; one moderately metastatic: T-47D; two poorly metastatic: MCF-7 and SK-Br-3). The results of real-time PCR showed that ITGα3 and ITGβ5 were highly expressed in MDA-MB-231 and MDA-MB-231BO cells but were lowly expressed in MCF-7, T-47D, and SK-Br-3 cells ($P < 0.01$, Fig. 4a). Pearson correlation analysis confirmed that ITGα3 and ITGβ5 were positively correlated with the metastatic and invasive potential of breast cancer cells ($r = 0.720$ and 0.631).

After screening three shRNA vectors, pLKO.1-shRNA-ITGα3-3 and pLKO.1-shRNA-ITGβ5-3 were identified as the most appropriate interfering plasmid for subsequent use (Fig. 4b). Following transfection with pcDH/ITGα3 or pcDH/ITGβ5, the expression of ITGα3 or ITGβ5 was significantly elevated in MCF-7 cells, whereas pLKO.1-shRNA-ITGα3 (ITGβ5)−3 effectively downregulated the expression of ITGα3 or ITGβ5 in MDA-MB-231 and MDA-MB-231BO cells ($P < 0.01$, Fig. 4c).

Osthole prevents ITGα3- or ITGβ5-induced cell migration and invasion of breast cancer cells

As shown in Fig. 5a, ITGα3 or ITGβ5 knockdown markedly restrained the migration speed of MDA-MB-231BO and MDA-MB-231 cells compared with parental cells with control vectors (shCtrl) at 24 and 48 h after scratching. A similar decrease in the migration speed of two highly metastatic cells was observed in the shCtrl + osthole and shITG + osthole groups ($P < 0.05$ or $P < 0.01$). After treatment with 10 μg/mL of osthole for 48 h, the mean migration rates of shCtrl-MDA-MB-231 and shCtrl-MDA-MB-231BO cells dropped from (51.64% ± 2.95%) to (20.00% ± 2.65%) and from (45.13% ± 3.33%) to (17.42% ± 2.06%), respectively. However, there was no difference in the migration rate between the shCtrl + osthole and shITG + osthole groups ($P > 0.05$, Fig. 5a). MCF-7 cells with ITGα3 or ITGβ5 overexpression demonstrated a higher migration rate than that of the vector at 48 h (ITGα3: 39.12% ± 0.02% or ITGβ5: 35.56%±0.01% *vs*. vector: 30.10% ± 0.02%, $P < 0.01$). By contrast, 10 μg/mL of osthole significantly inhibited the migration of MCF-7 cells with ITGα3-OE or ITGβ5-OE ($P < 0.01$, Fig. 5b).

Accordingly, the downregulation of ITGα3 or ITGβ5 impeded the invasiveness of MDA-MB-231BO and MDA-MB-231 cells from the upper chamber of transwell inserts ($P < 0.01$). Similarly, osthole

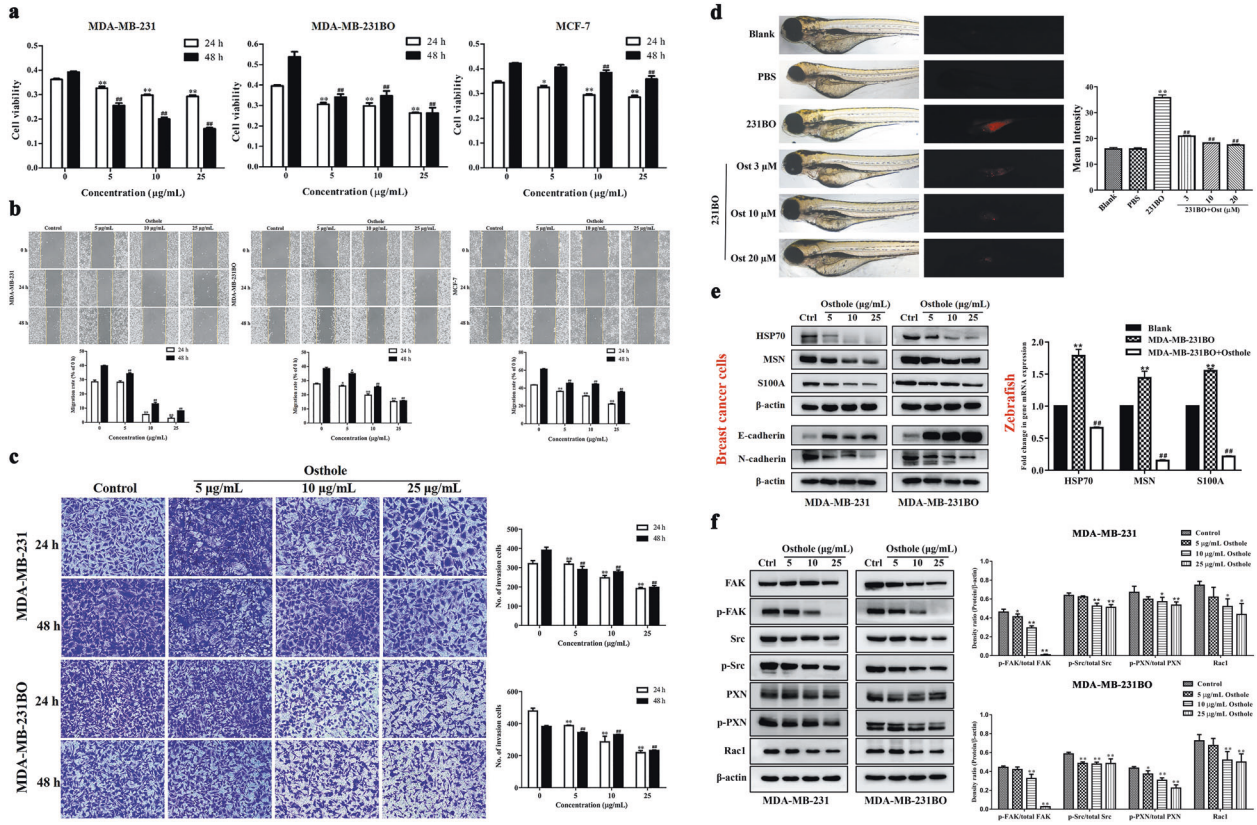

Fig. 2 Inhibitory effect of osthole at different concentrations on the proliferation, migration and invasion of highly metastatic breast cancer cells. a–c After treatment with osthole (5, 10, and 25 μg/mL) for 24 and 48 h, the cell proliferation, migration and invasion in both MDA-MB-231 and MDA-MB-231BO cells were analyzed by SRB, wound-healing, and transwell assays, respectively. Data were expressed as the mean ± SD for triplicate. $^{*}P < 0.05$, $^{**}P < 0.01$ *vs*. the control group for 24 h; $^{\#}P < 0.05$, $^{\#\#}P < 0.01$ *vs*. the control group for 48 h. Amplification factors: 100× for b and 200× for c. **d** A zebrafish breast cancer xenograft model was established by injecting Dil-labeled MDA-MB-231BO cells into the perivitelline cavity of each embryo. After treatment with different concentrations of osthole (3, 10, and 20 μmol/L) for 48 h, images of the disseminated tumor cells in the zebrafish body were captured using an inverted fluorescence microscope and the mean intensity of tumor cells was analyzed by ImageJ software. **e** Western blot was used to evaluate the effect of osthole on the expression of epithelial marker E-cadherin and the mesenchymal markers HSP70, MSN, S100A, and N-cadherin in highly metastatic breast cancer cells; real-time PCR was used to analyze the effect of osthole on the gene expression of HSP70, MSN, and S100A in the zebrafish breast cancer xenograft model. **f** Western blot was used to investigate the effect of osthole on the protein expression of FAK/Src/Rac1 signaling. Data were expressed as the mean ± SD for triplicate. $^{**}P < 0.01$ *vs*. the blank group; $^{\#\#}P < 0.01$ *vs*. the MDA-MB-231BO group. Ctrl: control; Ost: osthole.

(10 μg/mL) combined with empty vector or integrin knockdown also significantly reduced cell invasive ability compared to the shCtrl group ($P < 0.01$). Whereas, no difference was observed between the shCtrl + osthole and shITG + osthole groups ($P > 0.05$, Fig. 5c). The upregulation of ITGα3 or ITGβ5 expression promoted transmembrane invasion compared with the control in MCF-7 cells ($P < 0.05$, Fig. 5d). However, the promoting effect of ITGα3 or ITGβ5 on the invasive capability of MCF-7 cells was significantly prohibited with 10 μg/mL of osthole treatment for 48 h ($P < 0.05$). The number of invading cells was suppressed by 93.75% (ITGα3-OE) and 45.94% (ITGβ5-OE) (Fig. 5d).

We detected typical metastatic biomarkers in breast cancer cells following knockdown or overexpression of ITGα3 or ITGβ5. Real-time PCR and confocal immunefluorescence analysis showed that overexpression of ITGα3 or ITGβ5 induced a significant increase in the expression levels of HSP70, MSN, and S100A in MCF-7 cells. By contrast, knockdown of ITGα3 or ITGβ5 greatly reduced the expression levels of the above biomarkers in MDA-MB-231 and MDA-MB-231BO cells. After separate treatment with 10 μg/mL of osthole for 48 h, the mRNA levels of HSP70, MSN and S100A were downregulated by 4.26-, 3.04-, 3.39-fold for shCtrl-MDA-MB-231, 0.90-, 1.85-, 1.97-fold for shCtrl-MDA-MB-231-BO, 2.26-, 2.27-, 1.21-fold for MCF-7-ITGα3-OE, and 1.22-, 1.20-, 2.40-fold for MCF-7-ITGβ5-OE ($P < 0.01$, Fig. 5e). Moreover, osthole further decreased the mRNA levels of HSP70 and MSN in two high-metastatic cells expressing shITGα3 or shITGβ5 compared with their relative controls ($P < 0.05$, $P < 0.01$, Fig. 5e). Correspondingly, osthole reversed the increasing MFI values of HSP70, MSN and S100A proteins induced by ITGα3 or ITGβ5 in shCtrl-MDA-MB-231 and shctr-MDA-MB-231BO cells (Fig. 5f) or MCF-7-ITGα3-OE and MCF-7-ITGβ5-OE cells (Fig. 5g).

Osthole downregulates ITGα3- or ITGβ5-mediated downstream signaling pathway

We analyzed the effects of osthole on ITGα3 and ITGβ5-mediated downstream signaling in breast cancer cells by using shITGα3/shITGβ5 and ITGα3-OE/ITGβ5-OE transfectants, respectively. Changes in intergins activating downstream FAK/Src/Rac1 cascade contribute to cancer cell growth, motility and metastasis [32, 33]. Immunofluorescence detection revealed that knockdown of the two intergins decreased FAK, Src, PXN, p-PXN, and Rac1 protein levels in highly metastatic MDA-MB-231 and MDA-MB-231BO cells. However, the overexpression of ITGα3/ITGβ5 increased these protein levels in poorly metastatic MCF-7 cells (Fig. 6b, c).

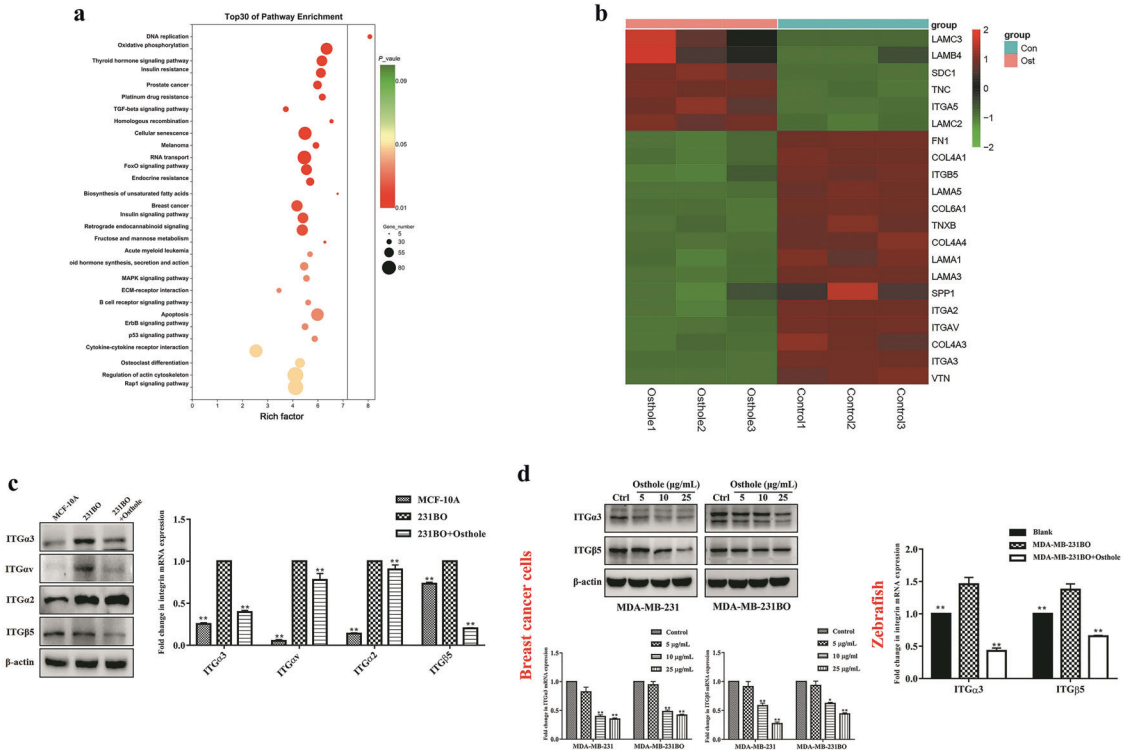

Fig. 3 Identification of candidate target genes of osthole in highly bone-metastatic breast cancer cells by RNA sequencing. a KEGG pathways enrichment analysis of differentially expressed genes (DEGs) in MDA-MB-231BO cells after osthole treatment. **b** Heatmap of DEGs between MDA-MB-231BO cells and MDA-MB-231BO + osthole cells (|log2 Fold Change| > 1, $P < 0.05$). **c** Identification of the candidate osthole-targeted genes using Western blot and real-time PCR. $^{**}P < 0.01$ *vs*. the MDA-MB-231BO group. **d** Regulatory effect of osthole on ITGα3 and ITGβ5 in highly metastatic breast cancer cells (MDA-MB-231 and MDA-MB-231BO) and the zebrafish breast cancer xenograft model induced by MDA-MB-231BO cells. Data were expressed as the mean ± SD for triplicate. For breast cancer cells, $^{*}P < 0.05$, $^{**}P < 0.01$ *vs*. the control group; for the zebrafish model, $^{**}P < 0.01$ *vs*. the MDA-MB-231BO group.

Treatment with 10 μg/mL osthole for 48 h efficiently inhibited the protein expression of FAK/Src/Rac1 signaling in MCF-7 cells with ITGα3-OE/ITGβ5-OE ($P < 0.01$). Similar to knockdown cells, osthole significantly reduced these transducin levels in MDA-MB-231 and MDA-MB-231BO cells with vector plasmid ($P < 0.01$). Compared with the shCtrl group, the decrease of MFI in shCtrl + osthole, shITGα3, shITGβ5, shITGα3 + osthole and shITGβ5 + osthole groups was 67.06%, 82.13%, 60.03%, 84.98% and 63.06% of FAK, 54.25%, 80.58%, 68.71%, 75.85%, and 69.33% of Src, 30.44%, 73.08%, 51.12%, 68.20% and 47.83% of PXN, 75.60%, 68.63%, 78.55%, 72.08% and 81.73% of p-PXN, and 83.69%, 78.82%, 65.52%, 73.78% and 75.18% of Rac1 (MDA-MB-231BO cells, $P < 0.01$, Fig. 6b, c). Osthole efficiently inhibited the protein expression of FAK/Src/Rac1 signaling in MCF-7 cells with overexpression of ITGα3 or ITGβ5 ($P < 0.01$, Fig. 6d). The mRNA levels of FAK, Src, PXN, and Rac1 were detected using real-time PCR, and the results were in accordance with their protein levels. Additionally, osthole further reduced the expression of these genes in MDA-MB-231 and MDA-MB-231BO cells expressing shITGα3 or shITGβ5 ($P < 0.05$ or $P < 0.01$, Fig. 6a).

DISCUSSION

In this study, the upregulation of ITGα3 and ITGβ5 was confirmed in metastatic breast cancer cells relative to normal mammary epithelial cells. The knockdown of ITGα3 or ITGβ5 significantly inhibited cell migration and invasion in highly metastatic MDA-MB-231 and its bone-tropic subtype MDA-MB-231BO cells, whereas the overexpression of ITGα3 or ITGβ5 enhanced the migratory and invasive capabilities of lowly metastatic MCF-7 cells. As a natural coumarin from *Fructus cnidii*, osthole could directly target ITGα3 or ITGβ5 to attenuate breast cancer cell migration and invasion through the suppression of the downstream FAK/Src/Rac1 signaling pathway.

Natural coumarins exist in various herbal medicines, including *Fructus cnidii*, *Fructus psoraleae*, and *Radix peucedani* [34]. Growing evidence has shown that natural coumarins possess noticeable anticancer activity against breast cancer, colon cancer, lung cancer, ovarian cancer, hepatocellular carcinoma, bladder carcinoma, leukemia, and other types of cancer [35–41]. Various studies indicate that osthole significantly inhibits cell proliferation by prohibiting angiogenesis [42], inducing apoptosis [43] and triggering cell autophagy [44]. Additionally, osthole showed great effects on the suppression of cancer metastasis through different mechanisms. A recent study reported that osthole inhibited NF-κB-mediated MMP-9 expression to reduce lung cancer cell invasion and migration [45]. Other studies also found that osthole blocked EMT-mediated metastatic ability in hepatocellular carcinoma, prostate and breast cancer [28, 46, 47].

Integrins are cell surface receptors that interact with ECM facilitating tumor growth and metastasis. In this study, RNA-sequence and in vitro validated assays revealed that ITGα3 and ITGβ5 were positively correlated with the metastatic and invasive potential of breast cancer cells, which might be the key targets of osthole in exerting anti-metastatic action. ITGα3 has been reported to be overexpressed in breast cancer cells with an invasive phenotype, and that human specimens showed a small number of ITGα3-positive cells located at the invasive front [48]. ITGα3 is determined to be a potential marker for enhancing EMT, invasion, and migration in breast cancer cells, which is positively regulated by MEK-ERK and PI3K/AKT signaling pathways [48, 49]. Loss of ITGα3 might disrupt an autocrine loop that could function to sustain metastatic growth [50]. ITGβ5 is another important

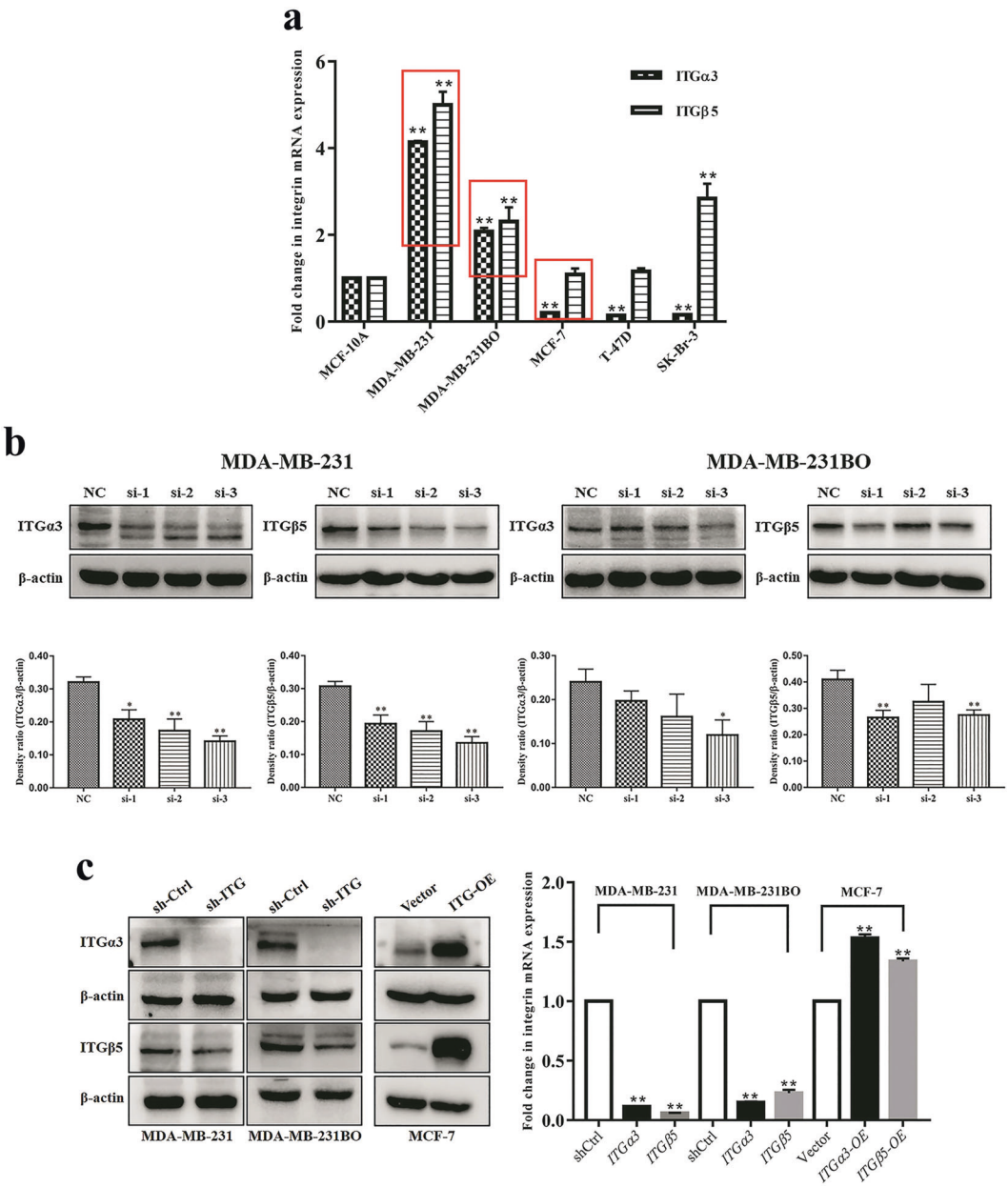

Fig. 4 Construction of stable ITGα3 or ITGβ5 knockdown and overexpression in human breast cancer cells. a The mRNA expression of ITGα3 and ITGβ5 in breast cancer cells with different metastatic capability. Data were expressed as the mean ± SD for triplicate. $^{**}P < 0.01$ *vs.* the MCF-10A group. **b** The determination of the most efficient shRNA interfering plasmid of ITGα3 and ITGβ5 in MDA-MB-231 and MDA-MB-231BO cells. $^{*}P < 0.05$, $^{**}P < 0.01$ *vs.* the negative control (NC). **c** The construction of ITGα3 or ITGβ5 knockdown cell lines (MDA-MB-231 and MDA-MB-231BO) and ITGα3 or ITGβ5 overexpression cell lines (MCF-7). $^{**}P < 0.01$ *vs.* the shCtrl or the vector group. shCtrl: control vectors.

regulator in promoting breast cancer metastasis. A study of 3D suspension cultures found that integrin β5 and Src promoted the initial attachment and spreading of TNBC cells to secondary organs after circulation during metastasis [51]. ITGβ5 and the downstream Src/NF-κB pathway in tumor cells for CXCR4/SDF1α-axis triggered lymph node premetastatic niche formation and mediated breast cancer metastasis [52]. Depletion of ITGβ5 in TNBC cells markedly reduced the growth, angiogenesis, migration, and proliferative capacities, and the re-expression of ITGβ5 rescued this phenotype [32].

Epithelial-mesenchymal transition (EMT) is an important process implicated in tumor invasion and metastasis. Notably, as an adhesion receptor on the cell surface, integrin participates in facilitating EMT process [53]. Some transcription factors such as STAT3, ZEB2, Twist1, and TAF4b were found to specifically upregulate the transcription of integrin mRNA (ITGβ6, ITGα5 and ITGα6), thus inducing migration, invasion and EMT in cancer cells [54–57]. In previous studies, osthole displayed a significant inhibitory effect on EMT by downregulating the expression of transcriptional factors Smad3, Snail1, Twist1, and STAT3 in renal cell carcinoma, prostate and gallbladder cancer [46, 58, 59]. Similarly, our results demonstrated that osthole could reverse ITGα3- or ITGβ5-induced EMT process by increasing epithelial markers (E-cadherin) and decreasing mesenchymal markers (HSP70, MSN, S100A, and N-cadherin) in highly metastatic breast cancer cells. Based on these finding, we will focus on the key transcription factors to further explore the molecular interaction between osthole and integrins in breast cancer.

In conclusion, osthole is shown to function as an anti-metastatic component in breast cancer. To the best of our knowledge, this

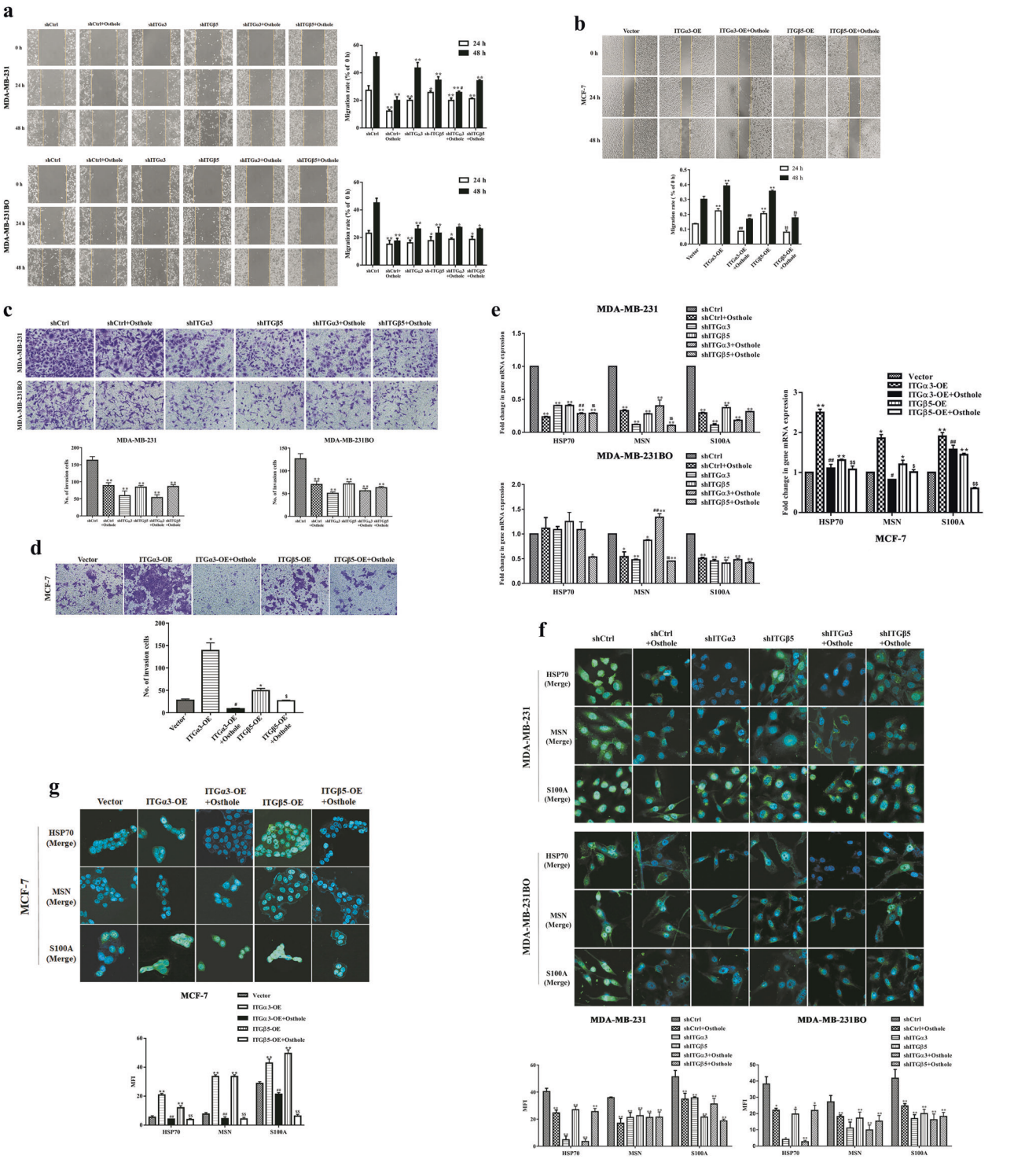

Fig. 5 Osthole prevents ITGα3- and ITGβ5-induced cell migration and invasion of highly metastatic breast cancer cells. MDA-MB-231 and MDA-MB-231BO cells with shITGα3 or shITGβ5, and MCF-7 cells with ITGα3-OE or ITGβ5-OE were treated with 10 μg/mL of osthole for 24 h or 48 h, respectively. **a**, **b** The migration of different breast cancer cells was determined by wound-healing assay. **a** $^{*}P < 0.05$, $^{**}P < 0.01$ *vs*. the shCtrl group; $^{\#}P < 0.05$ *vs*. the shITGα3 group. **b** $^{**}P < 0.01$ *vs*. the vector group; $^{\#\#}P < 0.01$ *vs*. the ITGα3-OE group; $^{\$\$}P < 0.01$ *vs*. the ITGβ5-OE group. **c**, **d** The invasion of different breast cancer cells was detected by Transwell assay. $^{*}P < 0.05$, $^{**}P < 0.01$ *vs*. the shCtrl or the vector group; $^{\#}P < 0.05$ *vs*. the ITGα3-OE group; $^{\$}P < 0.05$ *vs*. the ITGβ5-OE group. **e** The mRNA expression of metastasis-related biomarkers (HSP70, MSN and S100A) was evaluated by real-time PCR. $^{*}P < 0.05$, $^{**}P < 0.01$ *vs*. the shCtrl or the vector group; $^{\#}P < 0.05$, $^{\#\#}P < 0.01$ *vs*. the shITGα3 or the ITGα3-OE group; $^{\$}P < 0.05$, $^{\$\$}P < 0.01$ *vs*. the shITGβ5 or the ITGβ5-OE group. **f**, **g** The protein expression of metastasis-related biomarkers (HSP70, MSN and S100A) was analyzed by immunofluorescence assay. Scale bar = 20 μm. $^{*}P < 0.05$, $^{**}P < 0.01$ *vs*. the shCtrl or the vector group; $^{\#\#}P < 0.01$ *vs*. the ITGα3-OE group; $^{\$\$}P < 0.01$ *vs*. the ITGβ5-OE group. Amplification factors: 100× for **a** and **b**′ and 200× for **c** and **d**. shCtrl: control vectors; MFI: mean fluorescence intensity.

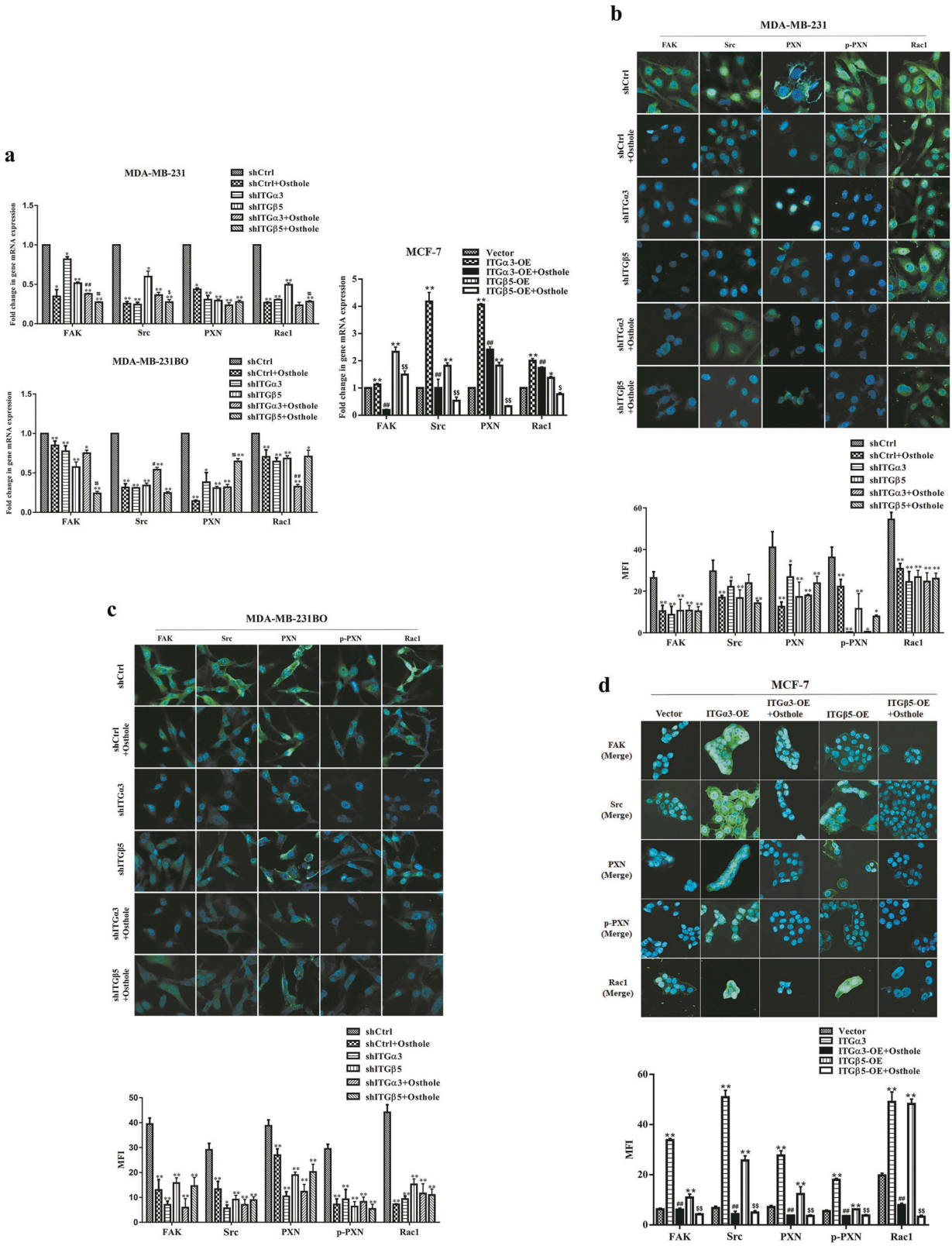

Fig. 6 Osthole suppresses ITGα3 and ITGβ5 downstream FAK/Src/Rac1 signaling. MDA-MB-231 and MDA-MB-231BO cells with shITGα3 or shITGβ5, and MCF-7 cells with ITGα3-OE or ITGβ5-OE were treated with 10 μg/mL of osthole for 48 h, respectively. **a** The mRNA expression of FAK, Src, paxillin (PXN), and Rac1 was evaluated by real-time PCR. $^{*}P < 0.05$, $^{**}P < 0.01$ *vs*. the shCtrl or the vector group; $^{\#}P < 0.05$, $^{\#\#}P < 0.01$ *vs*. the shITGα3 or the ITGα3-OE group; $^{\$}P < 0.05$, $^{\$\$}P < 0.01$ *vs*. the shITGβ5 or the ITGβ5-OE group. **b**–**d** The protein expression of FAK, p-FAK, Src, PXN, p-PXN, and Rac1 in MDA-MB-231 (**b**), MDA-MB-231BO (**c**), and MCF-7 (**d**) cells was analyzed by immunofluorescence assay. Scale bar = 20 μm. $^{*}P < 0.05$, $^{**}P < 0.01$ *vs*. the shCtrl or the vector group; $^{\#\#}P < 0.01$ *vs*. the ITGα3-OE group; $^{\$\$}P < 0.01$ *vs*. the ITGβ5-OE group. shCtrl: control vectors; MFI: mean fluorescence intensity.

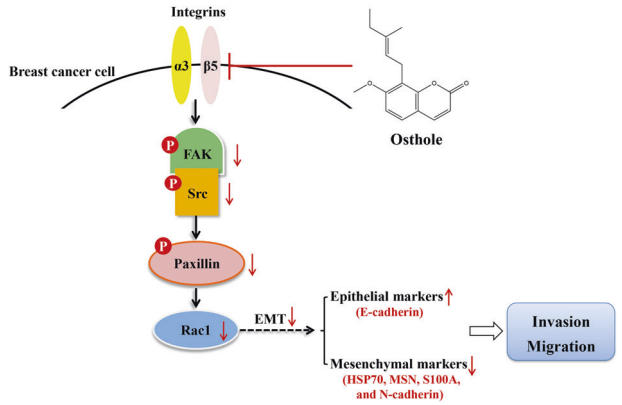

Fig. 7 Schematic representation of the antimetastatic mechanism of osthole on breast cancer by targeting the integrins. FAK: focal adhesion kinase; EMT: epithelial-mesenchymal transition.

study is the first to report that osthole directly targets ITGα3 or ITGβ5 and suppresses its downstream FAK/Src/Rac1 signaling in highly metastatic MDA-MB-231 and its bone-tropic subtype MDA-MB-231BO cells. This study provides some scientific evidence that osthole may be developed as a novel therapeutic drug for breast cancer metastasis (Fig. 7).

ACKNOWLEDGEMENTS

This work was supported by the National Natural Science Foundation of China (Nos. 81573973 and 81774308); the Natural Science Foundation of Shanghai (No. 20ZR1458600); the Outstanding Traditional Chinese Medicine Academic Leader Program of Shanghai (No. ZY (2018-2020)-RCPY-1011).

AUTHOR CONTRIBUTIONS

YQC, HYS, and JM conducted the main experiments; ZYZ carried out the zebrafish study; ZYL and YZ conducted the data analyses; SL provided guidance during the experiments; JYW and XHH designed the research and wrote the manuscript. All authors approved the final manuscript.

ADDITIONAL INFORMATION

Supplementary information The online version contains supplementary material available at https://doi.org/10.1038/s41401-021-00757-7.

Competing interests: The authors declare no competing interests.

REFERENCES

1. Sung H, Ferlay J, Siegel RL, Laversanne M, Soerjomataram I, Jemal A, et al. Global cancer statistics 2020: GLOBOCAN estimates of incidence and mortality worldwide for 36 cancers in 185 countries. CA Cancer J Clin. 2021;71:209–49.
2. DeSantis CE, Ma J, Goding Sauer A, Newman LA, Jemal A. Breast cancer statistics, 2017, racial disparity in mortality by state. CA Cancer J Clin. 2017;67:439–48.
3. Wang S, Li GX, Tan CC, He R, Kang LJ, Lu JT, et al. FOXF2 reprograms breast cancer cells into bone metastasis seeds. Nat Commun. 2019;10:2707.
4. Scully OJ, Bay BH, Yip G, Yu YN. Breast cancer metastasis. Cancer Genom Proteom. 2012;9:311–20.
5. Kozłowski J, Kozłowska A, Kocki J. Breast cancer metastasis - insight into selected molecular mechanisms of the phenomenon. Postepy Hig Med Dosw. 2015;69:447–51.
6. Desgrosellier JS, Cheresh DA. Integrins in cancer: biological implications and therapeutic opportunities. Nat Rev Cancer. 2010;10:9–22.
7. Rivera-Nieves J, Gorfu G, Ley K. Leukocyte adhesion molecules in animal models of inflammatory bowel disease. Inflamm Bowel Dis. 2008;14:1715–35.
8. Gilcrease MZ. Integrin signaling in epithelial cells. Cancer Lett. 2007;247:1–25.
9. Givant-Horwitz V, Davidson B, Reich R. Laminin-induced signaling in tumor cells. Cancer Lett. 2005;223:1–10.
10. Ungewiss C, Rizvi ZH, Roybal JD, Peng DH, Gold KA, Shin DH, et al. The microRNA-200/Zeb1 axis regulates ECM-dependent β1-integrin/FAK signaling, cancer cell invasion and metastasis through CRKL. Sci Rep. 2016;6:18652.
11. Das V, Kalyan G, Hazra S, Pal M. Understanding the role of structural integrity and differential expression of integrin profiling to identify potential therapeutic targets in breast cancer. J Cell Physiol. 2018;233:168–85.
12. Huang CF, Verhulst S, Shen Y, Bu YW, Cao Y, He YC, et al. AKR1B10 promotes breast cancer metastasis through integrin α5/δ-catenin mediated FAK/Src/Rac1 signaling pathway. Oncotarget. 2016;7:43779–91.
13. Flamini MI, Uzair ID, Pennacchio GE, Neira FJ, Mondaca JM, Cuello-Carrión FD, et al. Thyroid hormone controls breast cancer cell movement via integrin αv/β3/SRC/FAK/PI3-kinases. Horm Cancer. 2017;8:16–27.
14. Tai YL, Chu PY, Lai IR, Wang MY, Tseng HY, Guan JL, et al. An EGFR/Src-dependent β4 integrin/FAK complex contributes to malignancy of breast cancer. Sci Rep. 2015;5:16408.
15. Li WT, Liu ZJ, Zhao CL, Zhai LM. Binding of MMP-9-degraded fibronectin to β6 integrin promotes invasion *via* the FAK-Src-related Erk1/2 and PI3K/Akt/Smad-1/5/8 pathways in breast cancer. Oncol Rep. 2015;34:1345–52.
16. Ma Y, Wang LF, Xu ZY. Research progress on traditional Chinese medicine treatment of bone metastatic cancer pain. World Sci Tech Modern Trad Chin Med Mater Med. 2018;20:468–72.
17. Chen J. Clinical study on the treatment of "Wenshen Zhuanggu" method for bone metastatic pain in breast cancer. Master's dissertation, Shanghai: Shanghai University of Traditional Chinese Medicine; 2018.
18. Li JJ, Chen WL, Wang JY, Hu QW, Sun ZP, Zhang S, et al. Wenshen Zhuanggu Formula effectively suppresses breast cancer bone metastases in a mouse xenograft model. Acta Pharmacol Sin. 2017;38:1369–80.
19. Chen WL, Li JJ, Sun ZP, Wu CY, Ma J, Wang JY, et al. Comparative pharmacokinetics of six coumarins in normal and breast cancer bone-metastatic mice after oral administration of Wenshen Zhuanggu Formula. J Ethnopharmacol. 2018;224:36–44.
20. De Amicis F, Aquila S, Morelli C, Guido C, Santoro M, Perrotta I, et al. Bergapten drives autophagy through the up-regulation of PTEN expression in breast cancer cells. Mol Cancer. 2015;14:130.
21. Kleiner H, Reed M, DiGiovanni J. Naturally occurring coumarins inhibit human cytochromes P450 and block benzo[a]pyrene and 7,12-dimethylbenz[a]anthracene DNA adduct formation in MCF-7 cells. Chem Res Toxicol. 2003;16:415–22.
22. Wang XH, Xu CF, Hua YT, Cheng K, Zhang YZ, Liu J, et al. Psoralen induced cell cycle arrest by modulating Wnt/β-catenin pathway in breast cancer cells. Sci Rep. 2018;8:14001.
23. Oliveira CR, Spindola DG, Garcia DM, Erustes A, Bechara A, Palmeira-Dos-Santos C, et al. Medicinal properties of angelica archangelica root extract: cytotoxicity in breast cancer cells and its protective effects against in vivo tumor development. J Integr Med. 2019;17:132–40.
24. Shokoohinia Y, Jafari F, Mohammadi Z, Bazvandi L, Hosseinzadeh L, Chow N, et al. Potential anticancer properties of osthol: a comprehensive mechanistic review. Nutrients. 2018;10:36.
25. Park W, Park S, Song G, Lim W. Inhibitory effects of osthole on human breast cancer cell progression via induction of cell cycle arrest, mitochondrial dysfunction, and ER stress. Nutrients. 2019;11:2777.
26. Dai XX, Yin CT, Zhang Y, Guo GL, Zhao CG, Wang OC, et al. Osthole inhibits triple negative breast cancer cells by suppressing STAT3. J Exp Clin Cancer Res. 2018;37:322.
27. Yang DP, Gu TW, Wang T, Tang QJ, Ma CY. Effects of osthole on migration and invasion in breast cancer cells. Biosci Biotechnol Biochem. 2010;74:1430–4.
28. Hung CM, Kuo DH, Chou CH, Su YC, Ho CT, Way TD. Osthole suppresses hepatocyte growth factor (HGF)-induced epithelial-mesenchymal transition *via* repression of the c-Met/Akt/mTOR pathway in human breast cancer cells. J Agric Food Chem. 2011;59:9683–90.
29. Zhou ZY, Xiao Y, Zhao WR, Zhang J, Shi WT, Ma ZL, et al. Pro-angiogenesis effect and transcriptome profile of Shuxinyin formula in zebrafish. Phytomedicine. 2019;65:153083.
30. Kurozumi A, Goto Y, Matsushita R, Fukumoto I, Kato M, Nishikawa R, et al. Tumor-suppressive microRNA-223 inhibits cancer cell migration and invasion by targeting ITGA3/ITGB1 signaling in prostate cancer. Cancer Sci. 2016;107:84–94.
31. Hamidi H, Ivaska J. Every step of the way: integrins in cancer progression and metastasis. Nat Rev Cancer. 2018;18:533–48.
32. Wang JR, Liu B, Zhou L, Huang YX. MicroRNA-124-3p suppresses cell migration and invasion by targeting ITGA3 signaling in bladder cancer. Cancer Biomark. 2019;24:159–72.
33. Bianchi-Smiraglia A, Paesante S, Bakin AV. Integrin β5 contributes to the tumorigenic potential of breast cancer cells through the Src-FAK and MEK-ERK signaling pathways. Oncogene. 2013;32:3049–58.
34. Menezes JC, Diederich M. Translational role of natural coumarins and their derivatives as anticancer agents. Future Med Chem. 2019;11:1057–82.
35. Musa MA, Cooperwood JS, Khan MO. A review of coumarin derivatives in pharmacotherapy of breast cancer. Curr Med Chem. 2008;15:2664–79.

36. Saidu NE, Valente S, Bana E, Kirsch G, Bagrel D, Montenarh M. Coumarin polysulfides inhibit cell growth and induce apoptosis in HCT116 colon cancer cells. Bioorg Med Chem. 2012;20:1584–93.
37. Kumar M, Singla R, Dandriyal J, Jaitak V. Coumarin derivatives as anticancer agents for lung cancer therapy: a review. Anticancer Agents Med Chem. 2018;18:964–84.
38. Nordin N, Fadaeinasab M, Mohan S, Mohd Hashim N, Othman R, Karimian H, et al. Pulchrin A, a new natural coumarin derivative of enicosanthellum pulchrum, induces apoptosis in ovarian cancer cells via intrinsic pathway. PLoS One. 2016;11:e0154023.
39. Wang J, Lu ML, Dai HL, Zhang SP, Wang HX, Wei N. Esculetin. a coumarin derivative, exerts in vitro and in vivo antiproliferative activity against hepatocellular carcinoma by initiating a mitochondrial-dependent apoptosis pathway. Braz J Med Biol Res. 2015;48:245–53.
40. Haghighitalab A, Matin MM, Bahrami AR, Iranshahi M, Saeinasab M, Haghighi F. In vitro investigation of anticancer, cell-cycle-inhibitory, and apoptosis-inducing effects of diversin, a natural prenylated coumarin, on bladder carcinoma cells. Z Naturforsch C J Biosci. 2014;69:99–109.
41. Hejchman E, Taciak P, Kowalski S, Maciejewska D, Czajkowska A, Borowska J, et al. Synthesis and anticancer activity of 7-hydroxycoumarinyl gallates. Pharmacol Rep. 2015;67:236–44.
42. Yao F, Zhang LR, Jiang GR, Liu M, Liang GQ, Yuan Q. Osthole attenuates angiogenesis in an orthotopic mouse model of hepatocellular carcinoma *via* the downregulation of nuclear factor-κB and vascular endothelial growth factor. Oncol Lett. 2018;16:4471–9.
43. Che YL, Li J, Li ZJ, Li J, Wang S, Yan Y, et al. Osthole enhances antitumor activity and irradiation sensitivity of cervical cancer cells by suppressing ATM/NF-κB signaling. Oncol Rep. 2018;40:737–47.
44. Liang J, Zhou JL, Xu YQ, Huang XF, Wang XF, Huang WH, et al. Osthole inhibits ovarian carcinoma cells through LC3-mediated autophagy and GSDME-dependent pyroptosis except for apoptosis. Eur J Pharmacol. 2020;874:172990.
45. Kao SJ, Su JL, Chen CK, Yu MC, Bai KJ, Chang JH, et al. Osthole inhibits the invasive ability of human lung adenocarcinoma cells *via* suppression of NF-κB-mediated matrix metalloproteinase-9 expression. Toxicol Appl Pharmacol. 2012;261:105–15.
46. Wen YC, Lee WJ, Tan P, Yang SF, Hsiao M, Lee LM, et al. By inhibiting snail signaling and miR-23a-3p, osthole suppresses the EMT-mediated metastatic ability in prostate cancer. Oncotarget. 2015;6:21120–36.
47. Wu CY, Sun ZP, Guo BF, Ye YY, Han XH, Qin YN, et al. Osthole inhibits bone metastasis of breast cancer. Oncotarget. 2017;8:58480–93.
48. Shirakihara T, Kawasaki T, Fukagawa A, Semba K, Sakai R, Miyazono K, et al. Identification of integrin α3 as a molecular marker of cells undergoing epithelial-mesenchymal transition and of cancer cells with aggressive phenotypes. Cancer Sci. 2013;104:1189–97.
49. Zhang H, Cui XY, Cao AN, Li XL, Li LH. ITGA3 interacts with VASP to regulate stemness and epithelial-mesenchymal transition of breast cancer cells. Gene. 2020;734:144396.
50. Zhou B, Gibson-Corley KN, Herndon ME, Sun Y, Gustafson-Wagner E, Teoh-Fitzgerald M, et al. Integrin α3β1 can function to promote spontaneous metastasis and lung colonization of invasive breast carcinoma. Mol Cancer Res. 2014;12:143–54.
51. Park HJ, Helfman DM. Up-regulated fibronectin in 3D culture facilitates spreading of triple negative breast cancer cells on 2D through integrin β-5 and Src. Sci Rep. 2019;9:19950.
52. Gu Y, Liu YF, Fu L, Zhai LL, Zhu J, Han YM, et al. Tumor-educated B cells selectively promote breast cancer lymph node metastasis by HSPA4-targeting IgG. Nat Med. 2019;25:312–22.
53. Zhu C, Kong ZQ, Wang B, Cheng W, Wu AH, Meng X. ITGB3/CD61: a hub modulator and target in the tumor microenvironment. Am J Transl Res. 2019;11:7195–208.
54. Xu MY, Chen XH, Yin H, Yin LQ, Liu F, Fu YC, et al. Cloning and characterization of the human integrin β6 gene promoter. PLoS One. 2015;10:e0121439.
55. Nam EH, Lee Y, Park YK, Lee JW, Kim S. ZEB2 upregulates integrin α5 expression through cooperation with Sp1 to induce invasion during epithelial-mesenchymal transition of human cancer cells. Carcinogenesis. 2012;33:563–71.
56. Nam EH, Lee Y, Moon B, Lee JW, Kim S. Twist1 and AP-1 cooperatively upregulate integrin α5 expression to induce invasion and the epithelial-mesenchymal transition. Carcinogenesis. 2015;36:327–37.
57. Kalogeropoulou M, Voulgari A, Kostourou V, Sandaltzopoulos R, Dikstein R, Davidson I, et al. TAF4b and Jun/activating protein-1 collaborate to regulate the expression of integrin alpha6 and cancer cell migration properties. Mol Cancer Res. 2010;8:554–68.
58. Liu L, Mao J, Wang QF, Zhang ZW, Wu GZ, Tang QZ, et al. In vitro anticancer activities of osthole against renal cell carcinoma cells. Biomed Pharmacother. 2017;94:1020–7.
59. Zou TL, Wang HF, Ren T, Shao ZY, Yuan RY, Gao Y, et al. Osthole inhibits the progression of human gallbladder cancer cells through JAK/STAT3 signal pathway both in vitro and in vivo. Anticancer Drugs. 2019;30:1022–30.